Bone Reports 19 (2023) 101714

Contents lists available at ScienceDirect

Bone Reports

journal homepage: www.elsevier.com/locate/bonr

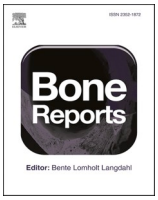

Three-dimensional morphometric analysis of cranial sutures – A novel approach to quantitative analysis

Ross Remesz [a], Tsolmonbaatar Khurelbaatar [a], Karyne N. Rabey [b,c], Michael R. Doschak [d], Dan L. Romanyk [a,e,*]

[a] Department of Mechanical Engineering, University of Alberta, Edmonton, AB, Canada
[b] Division of Anatomy, Department of Surgery, University of Alberta, Edmonton, AB, Canada
[c] Department of Anthropology, University of Alberta, Edmonton, AB, Canada
[d] Faculty of Pharmacy and Pharmaceutical Sciences, University of Alberta, Edmonton, AB, Canada
[e] School of Dentistry, University of Alberta, Edmonton, AB, Canada

ARTICLE INFO

Keywords:
Cranial suture
Morphology
Computed tomography
Image analysis
Linear interdigitation index

ABSTRACT

Objective: Differences in complexity of cranial suture forms on the endocranial (i.e., deep) and ectocranial (i.e., superficial) skull surfaces have been noted in the literature, indicating through thickness three-dimensional (3D) suture variability depending on the chosen section and necessity for considering the complete 3D structure in many cases. This study aims to evaluate the variability of suture morphology through the skull thickness using a rat model, and to provide more robust metrics and methodologies to analyze suture morphology.
Design: X-ray micro-computed tomographic (μCT) imaging methods were utilized in order to provide internal structure information. Methods were developed to isolate and analyze sutures widths and linear interdigitation index (LII) values on each adjacent offset transverse plane of the μCT datasets. LII was defined as the curved path length of the suture divided by the linear length between the ends of the region of interest. Scans were obtained on 15 female rats at ages of 16, 20, and 24 weeks ($n = 5$/age). Samples were imaged at 18 μm resolutions with 90 kV source voltage, 278 μA source amperage, and 0.7° increments. Suture widths and LII values were compared using a Kruskal-Wallis test.
Results: 3D variability in local suture widths within individuals, as well as through thickness variabilities in planar widths and LII was observed. Kruskal-Wallis tests for bulk through thickness averaged suture widths and LII were found to be statistically insignificant, despite clear geometric differences through suture thicknesses.
Conclusion: Although the bulk morphometric variability between age groups was found to be statistically insignificant, the 3D variability within individuals point to the importance of analyzing suture form using 3D metrics when studying suture development, response to functional activity, or morphometry in general.

1. Introduction

Craniofacial sutures are a network of soft tissues that serve a crucial role in the development and mechanical environment of the skull (Herring, 2008; Persson, 1995), acting as a growth site (Opperman, 2000) and strain sink (Herring, 2008). Sutures are typically comprised of structured collagen fibers, extracellular matrix (proteoglycans, fibers, and water) and vasculature (i.e., fibrous connective tissue) (Herring, 2008); their structure connects and integrates them into adjacent bones. Sutures adapt at cellular (Vij and Mao, 2006; Byron, 2006), and, subsequently, morphological (Rafferty and Herring, 1999; Herring and Ochareon, 2005) levels based on the loads experienced in vivo. Morphological adaptations of sutures to applied loading has been noted in the literature, where sutures that are compressed in vivo typically exhibit higher levels of interdigitation than sutures that are tensed (Herring and Ochareon, 2005; Markey et al., 2006). Researchers studying suture morphology are typically interested in exploring ex vivo properties of suture complexes (Maloul et al., 2013; Jaslow, 1990; Radhakrishnan and Mao, 2004), in vivo suture loads and loading conditions (Rafferty and Herring, 1999; Rafferty et al., 2019; Herring and

* Corresponding author at: Department of Mechanical Engineering, University of Alberta, 10-354 Donadeo Innovation Centre for Engineering, Edmonton, Alberta T6G 1H9, Canada.
E-mail address: dromanyk@ualberta.ca (D.L. Romanyk).

https://doi.org/10.1016/j.bonr.2023.101714
Received 29 May 2023; Received in revised form 16 September 2023; Accepted 19 September 2023
Available online 20 September 2023
2352-1872/© 2023 The Authors. Published by Elsevier Inc. This is an open access article under the CC BY-NC-ND license (http://creativecommons.org/licenses/by-nc-nd/4.0/).

Mucci, 1991), in vivo suture morphological adaptations (Herring, 2008; Peptan et al., 2008; Soh et al., 2018; Sun et al., 2004), developing and improving clinical applications (Guerrero-Vargas et al., 2019; Cohen, 1993; Mao et al., 2003; Bishara and Staley, 1987), or generating numerical and analytical modelling techniques involving suture complexity and mechanics (Jasinoski et al., 2010; Jasinoski and Reddy, 2012; Maloul et al., 2014; Liu et al., 2017).

Suture morphology is typically analyzed with visual/photographic analysis (Jayaprakash and Srinivasan, 2013; Byron, 2009; Nicolay and Vaders, 2006), histology (Sun et al., 2004; Burn et al., 2010; Willershausen et al., 2019; Savoldi et al., 2018), and/or X-ray imaging modalities (Markey et al., 2006; Savoldi et al., 2018; Savoldi et al., 2019; Wu et al., 2017; Khonsari et al., 2012). Skull dissection and visual methods allow for morphological analysis of the endocranial (i.e., interior/deep) and ectocranial (i.e., exterior/superficial) surfaces of sutures, but are limited to the skull surfaces. Histological methods allow researchers to see the cellular populations at the location of the histological slice, but are limited to planar information. X-ray modalities such as micro-computed tomography (μCT) can give information of sutures by a subtractive measure, assuming that the spaces between the bones on the scan are where the sutures reside.

Linear interdigitation index (LII) is a method for determining normalized planar suture complexity that has been used widely in the literature (Rafferty and Herring, 1999; Jasinoski et al., 2010; Savoldi et al., 2018; Savoldi et al., 2019; Markey and Marshall, 2007). Typically, LII is determined at a section plane, or from the endocranial or ectocranial surfaces of the skull. LII is determined by dividing the curved path length of the suture by the linear length between the ends of the region of interest, as shown in Eq. (1) (Savoldi et al., 2018; Savoldi et al., 2019). Although LII is commonly used to express levels of suture interdigitation, single plane expressions may not be a suitable way to convey the complexity of 3D spatially variable suture structures given potential variability through the skull thickness.

$$LII = \frac{l_{suture}}{l_{linear}} \tag{1}$$

Researchers have analyzed cranial suture morphology and composition using X-ray modalities (Markey et al., 2006; Savoldi et al., 2018; Savoldi et al., 2019; Wu et al., 2017; Khonsari et al., 2012). Subsequent analysis of the suture structure may be accomplished in a quantitative or qualitative manner. For instance, Savoldi et al. were interested in craniofacial suture morphology of swine where they utilized μCT with 25 μm resolution in order to quantitatively analyze the sutures (Savoldi et al., 2019). Their methods analyzed the middle most cross-sectional plane on both the perpendicular and parallel planes to the bone surface. Measures such as LII and width were analyzed, and results were grouped into facial, craniofacial, and cranial sutures. Although this method noted bulk differences in morphometric features from varying parts of the skull, and the 3D form of sutures was acknowledged by analyzing orthogonal planes, it did not provide insight to the degree of variability that is seen through the thickness of the skull in a single location or compare morphometric features between individuals. In another instance, Khonsari et al. used synchrotron μCT with 5 μm resolution in order to qualitatively investigate the structure of mouse and fish cranial sutures (Khonsari et al., 2012). The analysis method used was purely qualitative, noting progressive changes in interdigitation, uneven distributions of fibers and cells in the suture, and the presence of bone growth lines. Although these are interesting findings, quantifying their values would help other researchers find utility in these results. Although both quantitative and qualitative morphometric analysis has been performed with varying X-ray imaging modalities, studies interested in 3D suture morphometry are sparse in the literature and work focused on generating robust 3D morphometric data within sutures is not present.

Cranial suture sites are known to adapt in a number of ways throughout life, such as in response to mechanical state/loading with changes in fibre orientation and interdigitation (Herring, 2008); however, there has been limited quantitative work focused on 3D morphology of cranial sutures or justifying 2D analysis simplifications despite variable levels of interdigitation at the endocranial and ectocranial skull surfaces being qualitatively noted in the literature (Maloul et al., 2013; Maloul et al., 2014; Jayaprakash and Srinivasan, 2013). When pertaining to changes at a suture site with time, Henderson et al. were interested in age-dependent morphological and mechanical properties of sagittal sutures in rats (Henderson et al., 2005). The study was interested in morphometric features such as suture length, and width, as well as mechanics related to suture stiffness and in vivo quasi static strain in rats aged 2 to 60 days. They found that both geometric and mechanical properties are age dependent, however the analysis was conducted in a two-dimensional (2D) manner, and didn't provide any systematic methods for determining morphometric properties.

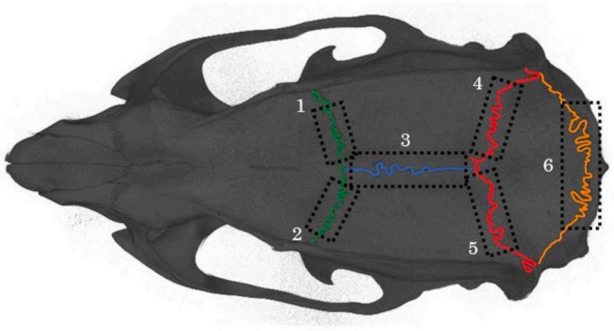

Fig. 1. A representative schematic showing sutures of interest, including the coronal (green), sagittal (blue), anterior lambdoid (red), and posterior lambdoid (orange). The approximate regions of interest are labeled as follows: 1, right-hand side coronal (C RHS); 2, left-hand side coronal (C LHS); 3, sagittal (S); 4, left-hand side anterior lambdoid (A RHS); 5, right-hand side anterior lambdoid (A LHS); and 6, posterior lambdoid (PL). (For interpretation of the references to color in this figure legend, the reader is referred to the web version of this article.)

The presented work intends to provide insight to how suture structures vary through skull thickness during development utilizing a novel quantitative analysis method to considering suture morphology. It is hypothesized that local and mean planar suture widths and LII will vary within an individual suture at different sections through the skull thickness. This is hypothesized because sutures experience complex loading conditions and have been shown to morphologically respond to their mechanical environment (Herring, 2008). It has generally been shown that sutures become more interdigitated in compression and straighter in tension (Herring, 2008). Bending has been shown to occur at suture sites (Rafferty et al., 2003), which could cause tension at one surface and compression at the other, driving morphological variability through the skull thickness. It is also hypothesized that statistically significant differences in mean suture width and LII between age groups will be present. Overall, the presented work aims to improve suture morphometric measurement methods and consider 3D morphometry to advance suture complexity quantification and provide 3D data for suture modelling.

2. Materials and methods

2.1. Data manipulation

Sprague–Dawley (SD) rats were used for all data collected in this study. These animals were originally part of a study interested in evaluating osteoarthritis progression, where all animal procedures were carried out in full compliance with the standards of the Animal Care and Use Committee of the University of Alberta (Panahifar et al., 2014). μCT scans were performed on 15 female rat carcasses euthanized at ages 16,

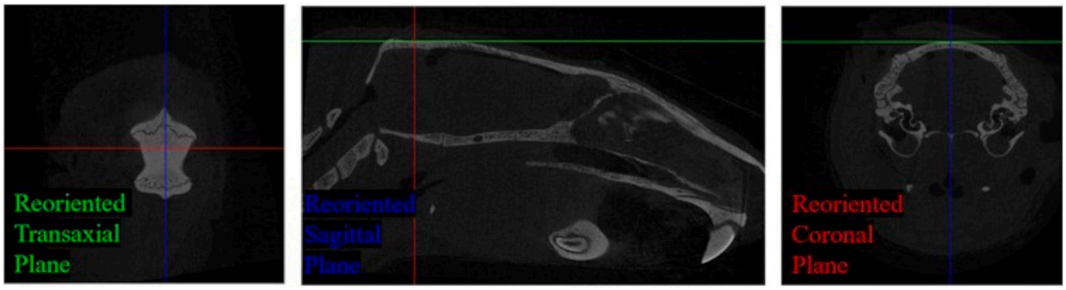

Fig. 2. A sample of the DataViewer interface used for reorienting datasets. A single plane of the output dataset for the posterior lambdoid suture is shown in the transaxial plane. The location of the transaxial image in this instance can be seen in the sagittal and coronal planes.

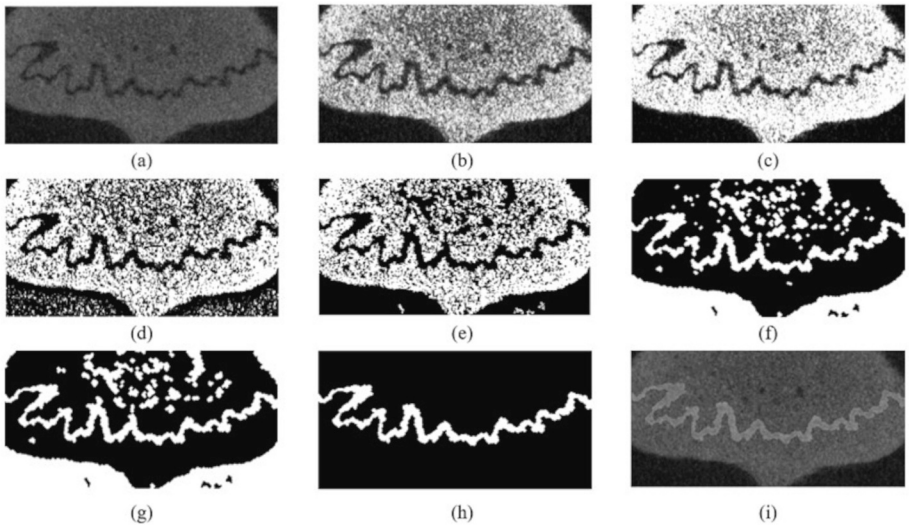

Fig. 3. Image processing of the posterior lambdoid suture from a 24-week-old female SD rat. (a) Cropped image of reoriented scan; (b) Histogram equalized; (c) Adjusted; (d) Binarized; (e) Filled; (f) Morphologically opened; (g) Segmentation, black to white; (h) Segmentation, white to black, final binary image; (i) Isolated suture area (65 % transparency) shown in (h) overlay on cropped image shown in (a).

20, and 24 weeks. An equal number of samples for each age group were analyzed (n = 5/age), and samples were scanned at 18 μm nominal resolutions with 90 kV source voltage, 278 μA source amperage, and 0.7° rotational steps using a Skyscan 1176 μCT (Bruker-SkyScan, Kontich, Belgium). The raw datasets were reconstructed using NRecon Version 1.6.3.3 (Bruker-SkyScan, Kontich, Belgium) and converted into orthotropic datasets. The cranial sutures of interest in this study were the coronal, sagittal, anterior lambdoid, and posterior lambdoid sutures, as shown on the 3D rendered skull in Fig. 1 which was generated using reconstructed μCT data and CTVox Version 2.0 (Bruker-SkyScan, Kontich, Belgium). The regions of interest for analysis were the right-hand side coronal (C RHS), left-hand side coronal (C LHS), sagittal (S), left-hand side anterior lambdoid (AL LHS), right-hand side anterior lambdoid (AL RHS), and posterior lambdoid (PL) sutures, marked on Fig. 1.

The reconstructed datasets were imported to DataViewer Version 1.4.3.2 (Bruker-SkyScan, Kontich, Belgium). All the reconstructed files were rotated using DataViewer in the coronal, sagittal, and transaxial planes in order to orient the μCT dataset to be approximately orthogonal to the suture of interest, as shown in Fig. 2. The reoriented output datasets contained a discrete set of images that show the skull cross section in the reoriented transaxial plane at 18 μm intervals through the entire dataset. Due to the curvature of the skull, a separate dataset was collected for the left and right portions of the coronal and anterior lambdoid sutures.

After the datasets were reoriented, they were converted to a binary form where the suture of interest was isolated using a method developed using MATLAB R2020A (MathWorks, Natick, USA). The range of planes in the reoriented transaxial dataset that contained the suture of interest were noted, and then copied to the corresponding MATLAB image processing folder. The process is shown using a representative plane of a 24-week-old posterior lambdoid suture in Fig. 3. First, a suitable cropping region of interest was determined by manually ensuring the suture of interest was in frame in the ectocranial-most and endocranial-most planes of the dataset. Each image in the stack was processed using an automated systematic image processing method developed for this application, where consistent parameter values were used to ensure consistent processing results. The processing started by cropping the ectocranial-most image obtained from the reoriented transaxial dataset to the cropped image shown in Fig. 3a. The cropped image was then equalized to increase the dynamic range and contrast of the image (Fig. 3b). The equalized image was then adjusted, where a consistent range of intensity values were used in order to further increase the contrast of the image (Fig. 3c). Next, the adjusted image was binarized (Fig. 3d) using a consistent threshold across all images so only the pixels corresponding to bones remained. Although this step eliminated some of the bone pixels and brought in stray pixels, the effect of lost pixels was the same across all sutures and animals since a consistent minimum threshold was used, and stray pixels within the suture were filled (Fig. 3e) based on the size (removed if the area is <30 pixels). The filled image was then inverted using built in MATLAB functions, then eroded and dilated using the same structuring element to smooth contours and eliminate thin protrusions from the suture outline while maintaining the outline size and shape (Fig. 3f). Erosion and dilation are morphological operations that, respectively, remove and add pixels on the object

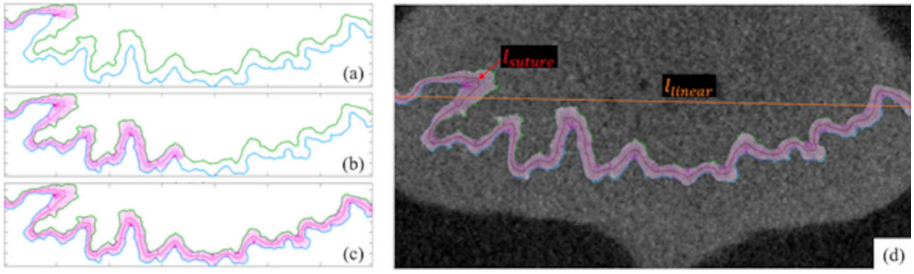

Fig. 4. Analysis of processed binary image of the posterior lambdoid suture from a 24-week-old female SD rat. (a) Analysis code in progress (early); (b) Analysis code in progress (middle); (c) Completed analysis; (d) Overlay of quantitative analysis on cropped image, suture length and linear length marked.

boundary; when performed in succession this operation is typically called morphological opening, which is useful in removing small objects from an image (stray pixels) while preserving the size and shape of larger objects (the suture). However, this step removed some parts of the suture and divided it into multiple parts, especially if the suture width was thin (<4 pixels). Thus, the separated suture parts were then manually connected, to ensure suture connectivity (Fig. 3g). Finally, the extraneous information was removed (Fig. 3h). An overlay of the isolated segmented suture outline (shown in Fig. 3f) at 65 % transparency on the cropped image (shown in Fig. 3a) can be seen in Fig. 3i. This process was repeated for each reoriented transaxial image by sequentially analyzing the 18 μm spaced images from ectocranial to endocranial ends of the dataset containing the suture of interest.

After processing and segmentation was complete, the isolated binary suture outlines were available for quantitative analysis for each of the 18 μm spaced images through the skull thickness. Each image was analyzed using a custom MATLAB script that generated lines using the top and bottom edges of the binarized segmented sutures. The script used a method that started on the left side of the suture image and traversed along the suture path measuring and storing local center point locations and widths between bone surfaces along the way (Fig. 4a and b). The script worked by taking a linear step of 1 pixel normal to the previous width's orientation from the width center point, then scanning a 90° range with 1° angular steps to find the closest distance between the top and bottom smoothed curves. The minimum distance between the top and bottom curve that intersected the location of the linear step taken normal to the previous width became the new local width. Once the new local width was found, the center of the local width was determined, and the process was repeated from the new center point. Once the entire suture was analyzed by this method, the center points were connected to create the suture path, where the length of this path is the suture length shown by the red centerline in Fig. 4c. An overlay of the suture analysis result (Fig. 4c) at 50 % transparency on the cropped image (shown in Fig. 3a) can be seen in Fig. 4d. This analysis method was iterated for each of the image planes in the reoriented transaxial dataset.

2.2. Data analysis

Data analysis began with the data closest to the ectocranial side and worked iteratively through the dataset until it reached the endocranial side. The script determined local suture widths, average planar widths, planar LII, mean suture widths, and mean suture LII.

Planar LII was found as a single measure for each plane of the reoriented μCT datasets by dividing the path length of the suture by the linear length between the end points as previously discussed and shown in Eq. (1). The local planar LII values can be expressed mathematically as $LII_{i,j}$, where i represents the specific sample that the local planar LII values were determined from (e.g., i = BML-3), and j represents the specific plane that the local planar LII values were determined at (e.g., ectocranial $j = 1$, endocranial $j = n$). The mean suture LII for an individual suture, $\overline{LII}_i$, was determined from the planar LII data using Eq. (2).

$$\overline{LII}_i = \frac{\sum_{j=1}^{n} LII_{i,j}}{n} \tag{2}$$

Local widths were computed along the suture path as shown in pink in Fig. 4, where each local width, $W_{i,j,k}$, was specific to a singular center point along the traversed suture path between the opposing bone fronts - where i represents the specific sample that the local widths were determined from, j represents the specific plane that the local width was determined at (e.g., ectocranial $j = 1$, endocranial $j = n$), and k represents the location along the suture path that the local width was determined at (e.g., left hand side (LHS) starting point $k = 1$, right hand side (RHS) end point $k = m$). The local widths were used to determine the mean planar width, $\overline{W}_{i,j}$, using Eq. (3). The mean planar widths were then used to determine the mean suture width, $\bar{W}_i$, using Eq. (4).

$$\overline{W}_{i,j} = \frac{\sum_{k=1}^{m} W_{i,j,k}}{m} \tag{3}$$

$$\bar{W}_i = \frac{\sum_{j=1}^{n} \overline{W}_{i,j}}{n} \tag{4}$$

A Kruskal-Wallis test was used to determine if there was statistically significant variability between age groups for each suture with respect to suture LII and width. The mean values for each suture LII and width, as described above in Eqs. (2) and (4), were utilized for comparison from each animal within its respective age group. The Kruskal-Wallis test was selected for this analysis due to the small sample sizes and inability to confirm normal distributions and equal variance among the populations. The null and alternative hypotheses used for the Kruskal-Wallis tests were as follows:

Suture LII Kruskal-Wallis:

- $H_{0,LII}$: There is no difference in median suture LII between the age groups.
- $H_{1,LII}$: There is a difference in median suture LII between the age groups.

Suture width Kruskal-Wallis:

- $H_{0,W}$: There is no difference in median suture width between the age groups.
- $H_{1,W}$: There is a difference in median suture width between the age groups.

The analysis was completed using 95 % confidence level, and 2 degrees of freedom due to the 3 age groups. Due to the different sample sizes of age groups in the posterior lambdoid suture, Eq. (5) was used to determine the test statistic, H.

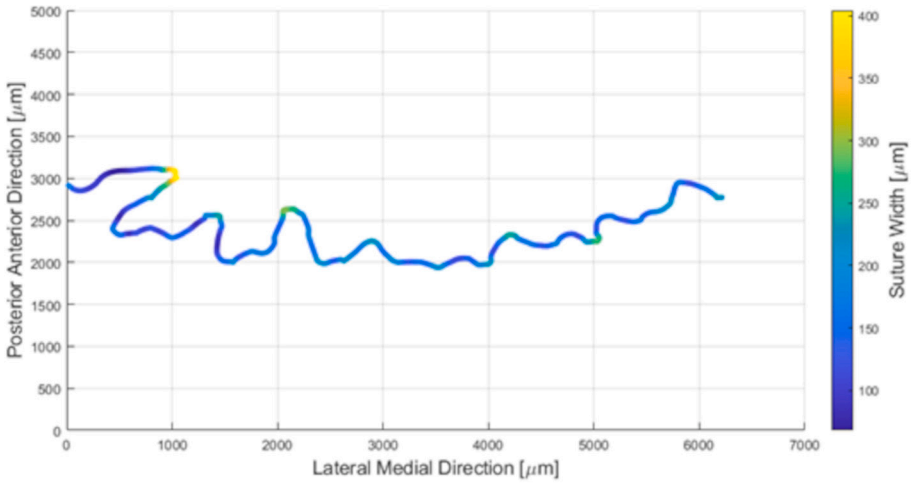

Fig. 5. Representative local planar widths along planar suture outline of the posterior lambdoid suture from a 24-week-old female SD rat.

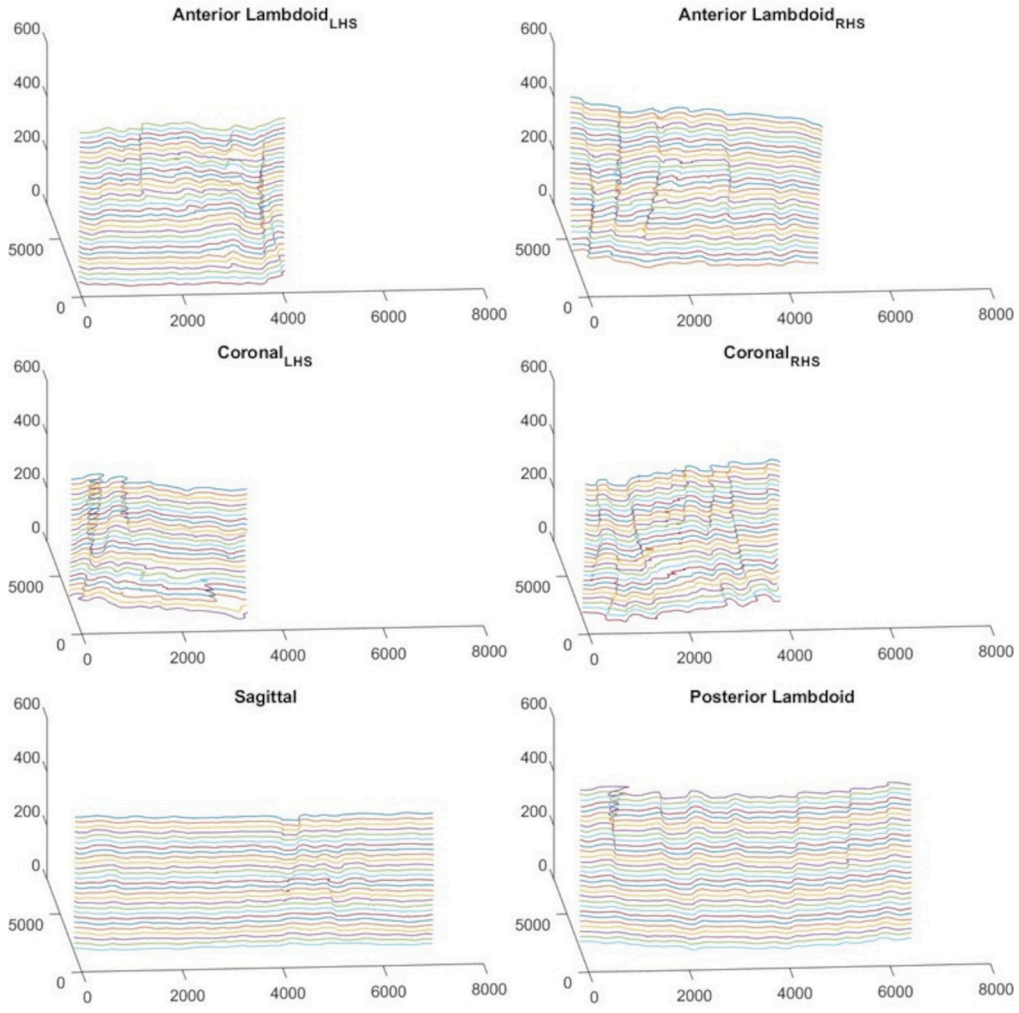

Fig. 6. Representative 3D centerlines of suture regions of interest from a single sample, scale is in μm. LHS = left-hand side, RHS = right-hand side.

$$H = (N-1)\frac{\sum_{i=1}^{g} n_i(\bar{r}_i - \bar{r})^2}{\sum_{i=1}^{g}\sum_{j=1}^{n_i}(r_{ij} - \bar{r})^2} \quad (5)$$

where, N is total number of observations across all groups, g is the number of groups, n_i is the number of observations in group i, r_{ij} is the rank (among all observations) of observation j from group i, $\bar{r}_i = \frac{\sum_{j=1}^{n_i} r_{ij}}{n_i}$ is the average rank of all observations in group i, and $\bar{r} = \frac{1}{2}(N+1)$ is the average of all the r_{ij}.

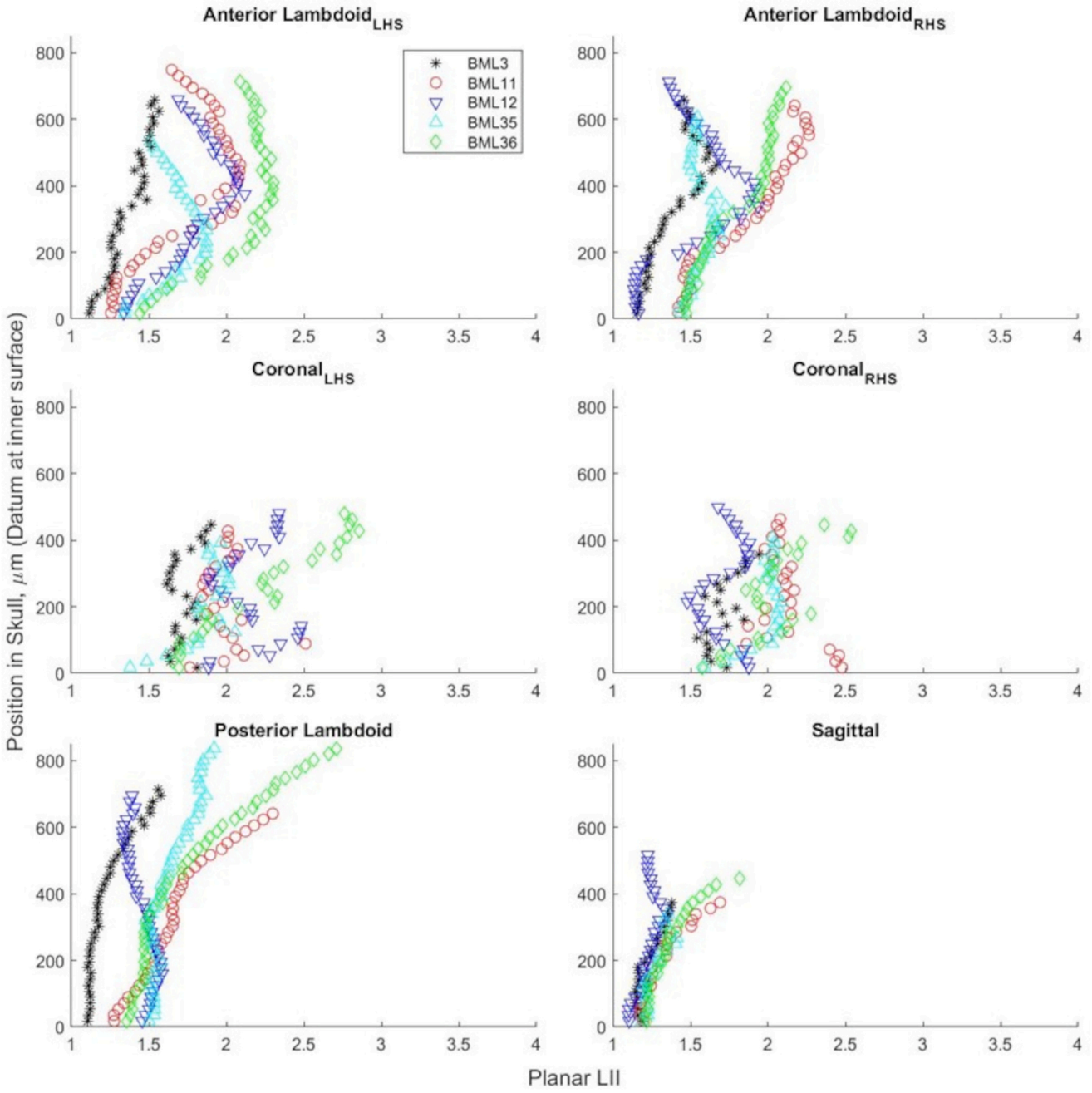

Fig. 7. 16-week-old rats: Planar linear interdigitation index (LII). LHS = left-hand side, RHS = right-hand side.

3. Results

3.1. Local planar widths

The local planar widths were found at each center point location as mentioned in the Materials and methods section. Fig. 5 shows the local width distribution along the same plane of the representative 24-week-old posterior lambdoid suture shown in Figs. 3 and 4. On a qualitative note regarding width along the suture path for a given plane, it generally appeared that the maximum local widths were noted at locations where the suture changed direction, and the minimum local widths were found in comparatively straighter running regions of the suture.

3.2. Planar LII and mean planar width

Representative plots of the 3D centerline paths of the six regions of interest in the same representative specimen shown previously are displayed in Fig. 6. These plots qualitatively show the suture centerline path variability as the planar position in the skull thickness changes. The anterior lambdoid, coronal, sagittal, and posterior lambdoid sutures centerlines all vary through the skull thickness, showing a dependence of planar suture form with position in the skull thickness. Due to a single posterior lambdoid sample being out of frame on a scan, a sample size $n = 4$ was used for the 24-week-old posterior lambdoid datasets.

Quantitative planar LII data shown through the skull thickness of the 16, 20, and 24-week-old rats can be found in Figs. 7, 8, and 9 respectively. Variations of LII through the thickness of a single specimen were found to range from 20.5 %–115.4 % for the anterior lambdoid suture

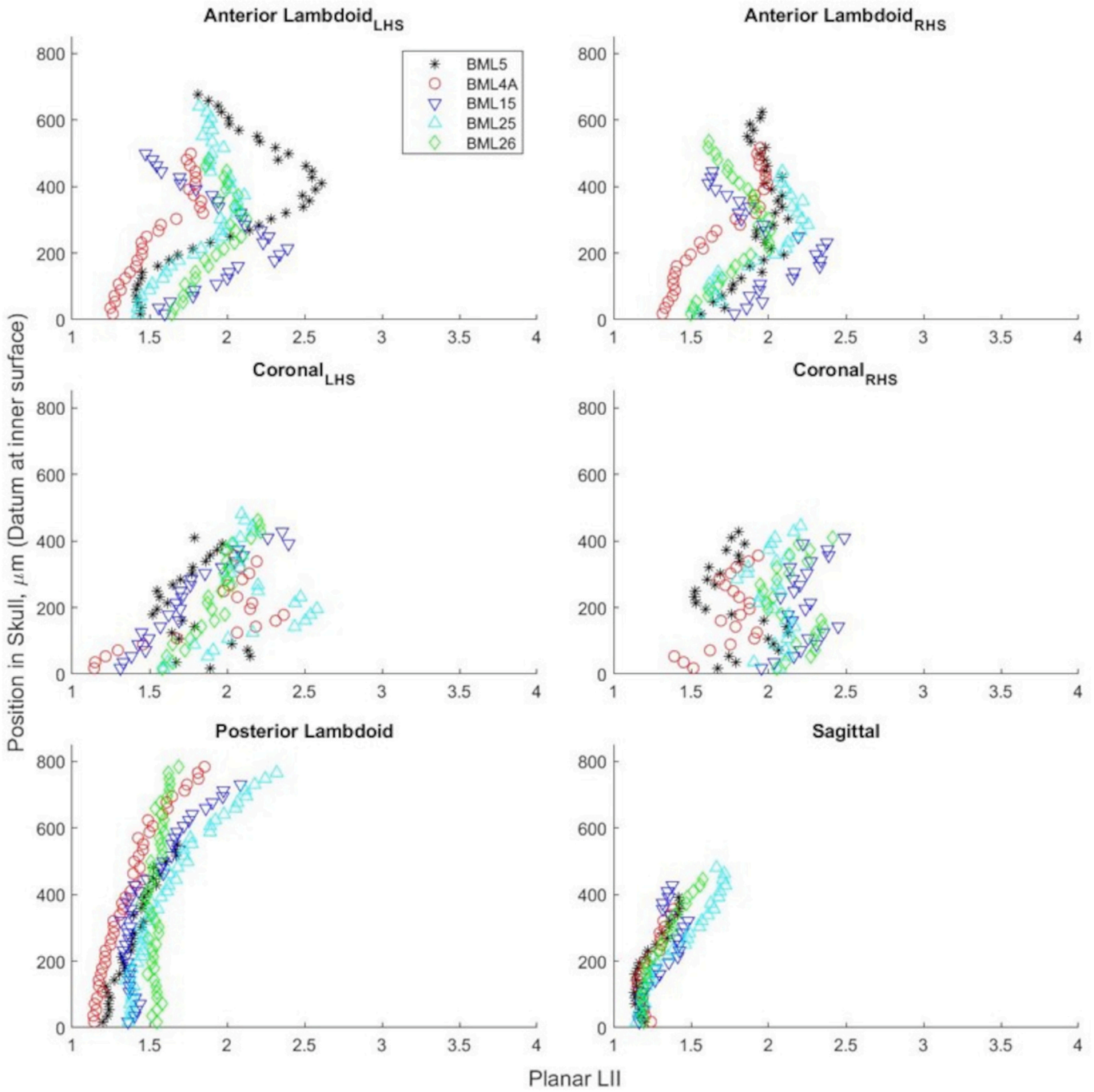

Fig. 8. 20-week-old rats: Planar linear interdigitation index (LII). LHS = left-hand side, RHS = right-hand side.

samples, 17.8 %–107.1 % for the coronal suture samples, 15.8 %–62.5 % for sagittal suture samples, and from 9.5 %–109.7 % for posterior lambdoid suture samples.

The mean planar width data provides quantitative information through the skull thickness of the 16, 20, and 24-week-old rats, shown in Figs. 10, 11, and 12 respectively. Variations of mean planar width through the thickness of a single specimen were found to range from 24.1 %–180.5 % for the anterior lambdoid suture samples, 14.8 %–136.7 % for the coronal suture samples, 15.3 %–99.7 % for sagittal suture samples, and from 17.4 %–61.6 % for posterior lambdoid suture samples.

3.3. Mean suture LII and width

The mean suture LIIs and mean suture widths of the 6 regions of interest analyzed can be found in Figs. 13 and 14 respectively. The mean suture LII appears to be constant between the age groups for the coronal, sagittal, and posterior lambdoid sutures. The anterior lambdoid suture qualitatively appears to have increased levels of mean suture LII with increased age; however, the statistical significance of this trend will be explored.

The results of the Kruskal-Wallis test of the suture LII and suture widths between the age groups are shown in Table 1. The Chi-Square (χ^2) value was determined to be $\chi^2 = 5.991$ from the Chi-Square Distribution using 2 degrees of freedom, and 95 % confidence level. With the exception of the suture LII of the right-hand side of the anterior

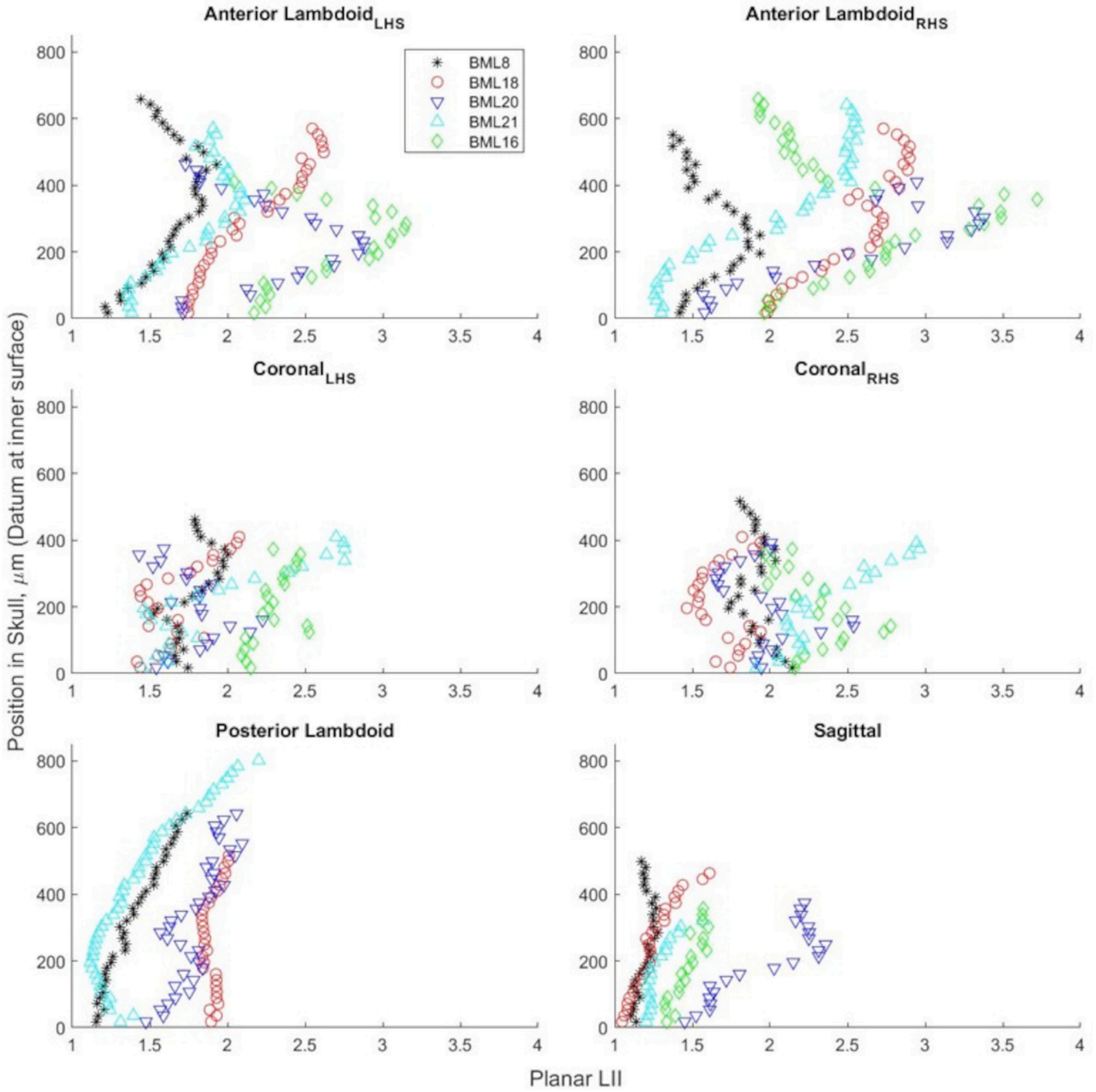

Fig. 9. 24-week-old rats: Planar linear interdigitation index (LII). LHS = left-hand side, RHS = right-hand side.

lambdoid suture, all of the test statistic values determined from the statistical analysis showed no significant difference among the three age groups in suture LII or width. This largely points to no significance in age with respect to suture LII, and points to no significance of age with respect to suture width.

Since the aforementioned Kruskal-Wallis tests surrounding age differences for the same suture showed no significant differences, it was then desirable to pool the results for sutures across ages to study differences between sutures. In doing so, the subsequent analysis would aim to demonstrate the potential of the developed methods to quantitatively discern differences in 3D suture geometry. An additional Kruskal-Wallis test was used to determine if statistical differences existed between sutures in terms of LII and width. The mean values for each suture LII and width were averaged across all ages, and the Kruskal-Wallis test evaluated the difference between sutures regardless of the age. The null and alternative hypothesis used for testing differences between sutures were:

Suture LII Kruskal-Wallis between sutures:

- $H_{0,LII}$: There is no difference in median suture LII between sutures
- $H_{1,LII}$: There is a difference in median suture LII between sutures

Suture width Kruskal-Wallis between sutures:

- $H_{0,W}$: There is no difference in median suture width between sutures
- $H_{1,W}$: There is a difference in median suture width between sutures

This analysis was conducted at a 95 % confidence level, and five

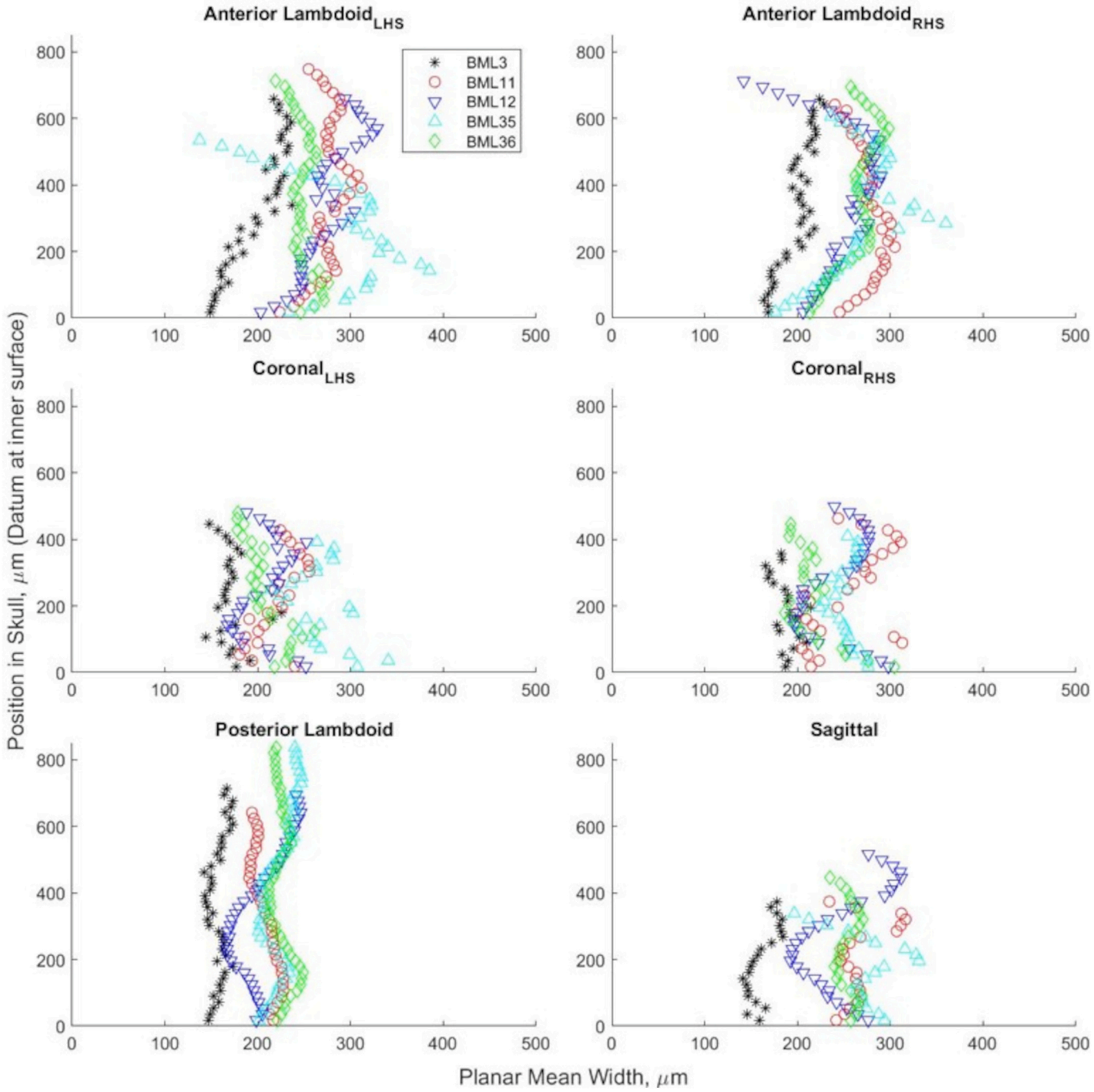

Fig. 10. 16-Week-old rats: Mean planar widths. LHS = left-hand side, RHS = right-hand side.

degrees of freedom based on the six different suture sites. The Kruskal-Wallis test was followed by post hoc multiple non parametric comparisons with Dunn-Sidák adjustment (Dunn, 1961; Šidák, 1967; Sheskin, 2011) for the cases where the null hypothesis was rejected.

The results of the Kruskal-Wallis test comparing LII and width between sutures showed that there were significant differences between sutures in terms of suture LII ($p < 0.01$); however, there was no difference between sutures in terms of suture width ($p > 0.05$). The p value of the post hoc multiple nonparametric comparisons of suture LII are listed in Table 2. The multiple nonparametric comparisons showed that there were significant differences between posterior lambdoid and coronal sutures, between anterior lambdoid and sagittal sutures, and between sagittal and coronal sutures. Other pairs of sutures did not show significant differences between them.

4. Discussion

Representatively and quantitatively conveying cranial suture complexity is challenging due to the 3D variable structure concealed by adjacent bones. A primary focus of this study was to develop methods for quantitatively analyzing X-ray μCT images of the cranial suture at different locations to evaluate their LII and width through bone thickness. Development of these methods advances the literature surrounding cranial suture morphometrics by presenting a systematic method through which sutures can be quantitatively compared when studying differences/changes in a range of applications. Using these methods, it was then of interest to compare cranial suture changes with age in a rat model. Planar and mean suture LII as well as local, mean planar, and mean suture widths were determined for six regions of interest on 15 rats

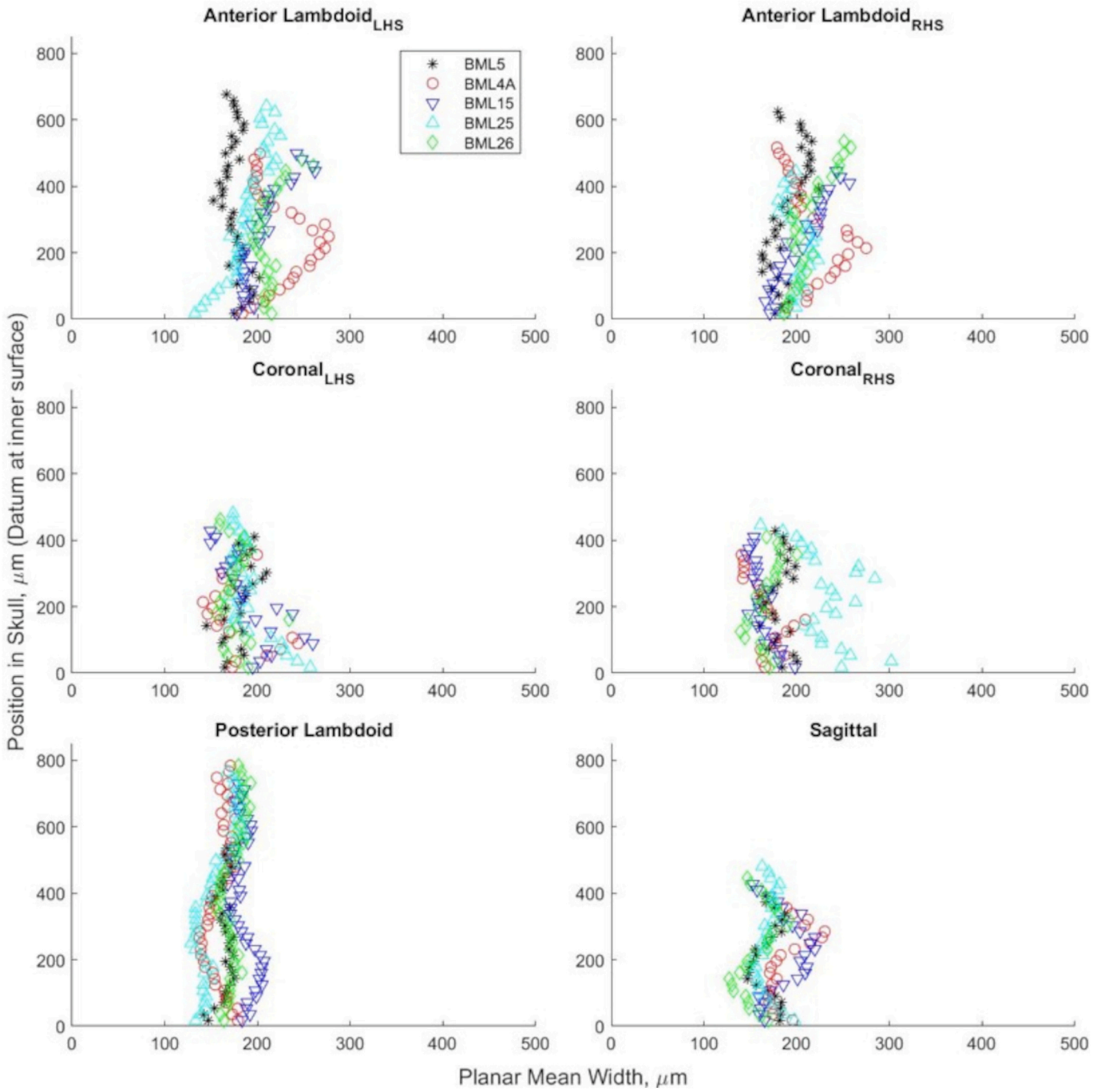

Fig. 11. 20-Week-old rats: Mean planar widths. LHS = left-hand side, RHS = right-hand side.

from three age groups. This provided 3D information regarding suture complexity and width trends through skull thickness. The methods demonstrated in this manuscript and the results are useful to researchers interested in suture development, relating suture mechanics to morphology, and/or modelling suture mechanics.

Cranial sutures are typically considered as 2D structures when modelled (Jasinoski et al., 2010; Jasinoski and Reddy, 2012; Liu et al., 2017) and morphologically analyzed (Rafferty and Herring, 1999; Savoldi et al., 2018). Furthermore, when the geometry is modelled, they are commonly represented as having a constant width and a normal sinusoidal morphology (Jasinoski et al., 2010; Jasinoski and Reddy, 2012). There have been models developed that incorporate irregularities in suture path, however constant width and 2D assumptions are still in place (Liu et al., 2017). The results of this work showed substantial local and mean planar width variability within sutures. This supports part of the overall hypothesis of this study, that width variability is exhibited within sutures; variability between sutures is also evident by comparing the quantitative data presented in Figs. 10 to 12. The mean planar sagittal suture widths measured in this study (142 μm–357 μm) are similar to results of Henderson et al., where they found rat sagittal suture widths of approximately 100 μm–450 μm, validating the results of this work (Henderson et al., 2005). The results indicate that if approximate suture widths are of interest, an average of multiple surface suture width measurements could represent the entire sagittal suture in rats.

The current work also presented quantitative through-thickness LII data, demonstrating planar LII variability of up to 115.4 % through the thickness of a single specimen. Results of this work support the hypothesis that LII may spatially vary through the skull thickness within a

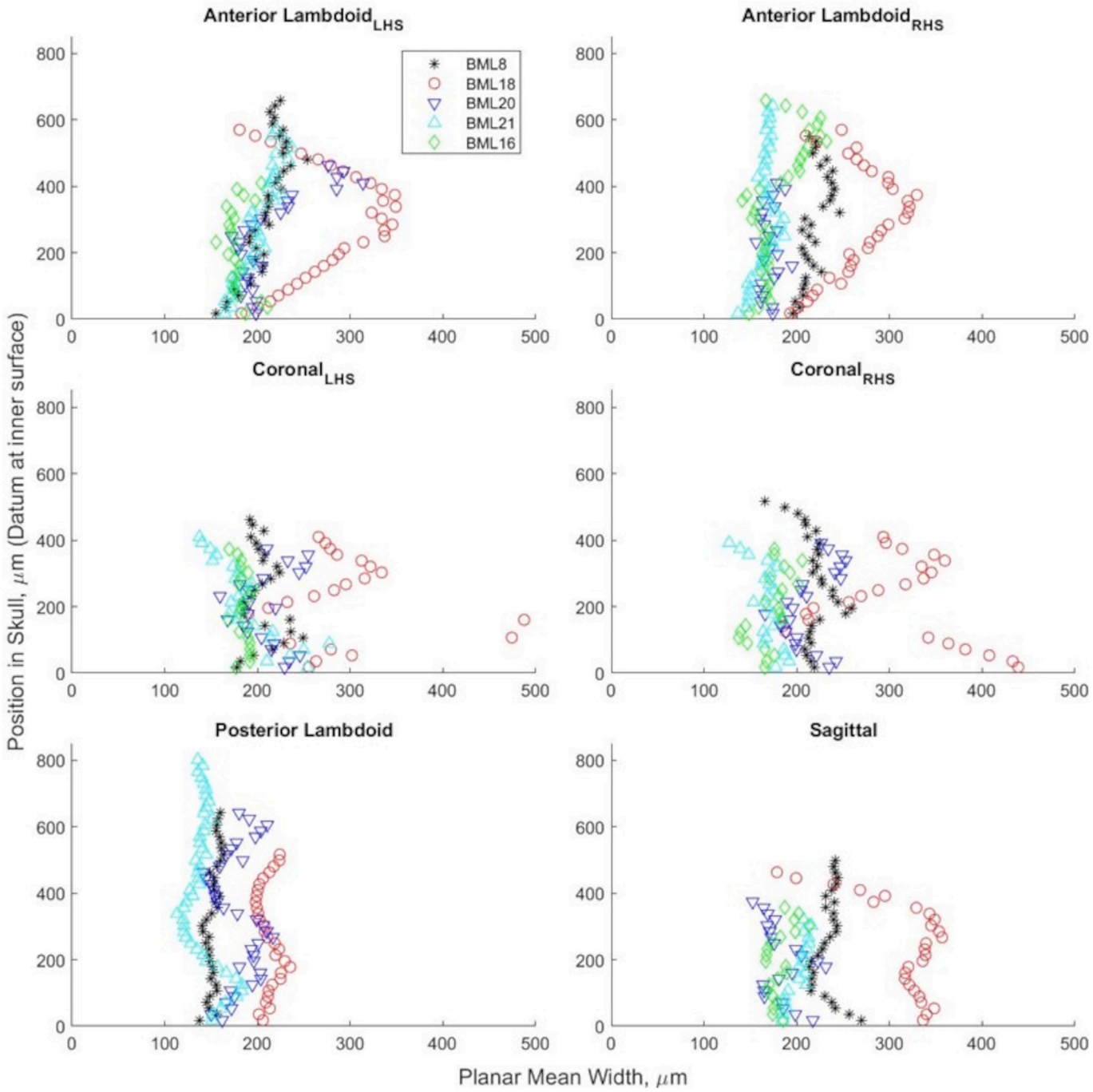

Fig. 12. 24-Week-old rats: Mean planar widths. LHS = left-hand side, RHS = right-hand side.

single suture and variability between sutures is also evident by comparing the quantitative data presented in Figs. 7 to 9. The statistical results of the Kruskal-Wallis test did not support the hypothesis that suture LII, and width will vary between age groups of 16 to 24 weeks. Although there was some variability shown between ages, the results in most instances were found to be statistically insignificant. When interpreting the lack of differences, it is suspected that since rats considered in this study were nearing the end of their skeletal maturity and within a tight age range of 8 weeks, there may have been less drastic changes (Hughes and Tanner, 1970). It is anticipated that considering younger rats undergoing increased skull growth/development or substantially older rats well outside the age range considered here may have produced larger differences showing statistical significance.

The secondary analysis comparing differences between sutures showed that there are statistically significant differences between sutures in terms of LII, but did not support the hypothesis there are statistically significant differences between sutures in terms of width. These results also further confirmed the evident differences between sutures depicted in Figs. 7 to 9. The lack of difference among different sutures in terms of suture width showed that the width is approximately constant across the investigated sutures despite the significant difference in terms of suture LII. This finding is in line with the theoretical conjecture that the suture width is regulated by a subsystem where the center region of sutures is rich in antiosteogenic factors whereas the outer region is rich in pro-osteogenic factors (Yu et al., 2004). While discrepancies in geometry between sutures in different locations may in some ways be expected due to different mechanical states leading to varied adaptations, the outcome of this analysis elucidates the utility of developed

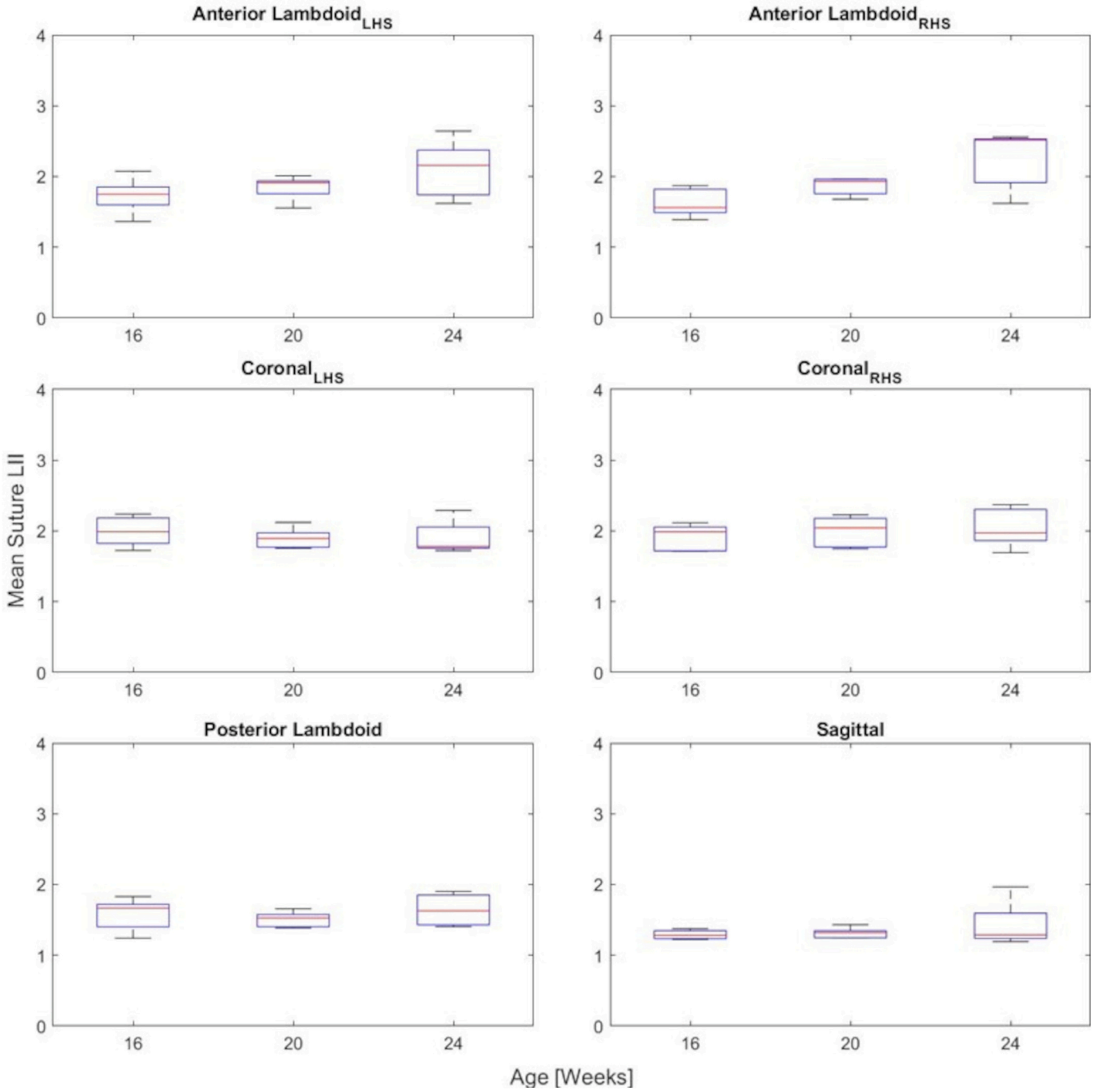

Fig. 13. Mean suture linear interdigitation index (LII) boxplots for suture regions of interest, grouped by age (16, 20, 24 week-of-age). LHS = left-hand side, RHS = right-hand side.

methods in quantitatively comparing suture morphometric quantities. As previously discussed, future work should focus on utilizing similar methods in exploring larger age ranges (i.e. considering both younger and older groups) to better explore morphometric changes in sutures.

The results of this work indicate that rat cranial suture width and LII can be variable through the thickness of the skull. This variability could have effects on studies that rely on measuring, characterizing, or modelling the morphological form of sutures. Since the through-thickness distributions of width and LII were not present in every suture, it is recommended that sutures be analyzed quantitatively to ensure there is no significant through thickness variability. If no significant variability is found from the endocranial and ectocranial surfaces, planar analysis of the suture may be appropriate and justifiable depending on the study objectives. The methods presented in this study could be employed when analyzing suture response to loading, as they would provide a high-resolution displacement map of how sutures are reacting if the subject is scanned before and after loading. The methods could also be utilized in studies interested in suture development and functional alterations by providing 3D morphological data which may also be linked to mechanical state through mechanical simulations.

This study did have several limitations. The small sample size for each suture region of interest per age group could certainly be improved with a higher number. The age groups analyzed were all near the final period of a rats skeletal maturity (Hughes and Tanner, 1970), future work should consider a wider age range in order to track full suture development. The analysis also did not consider the surfaces of the skull,

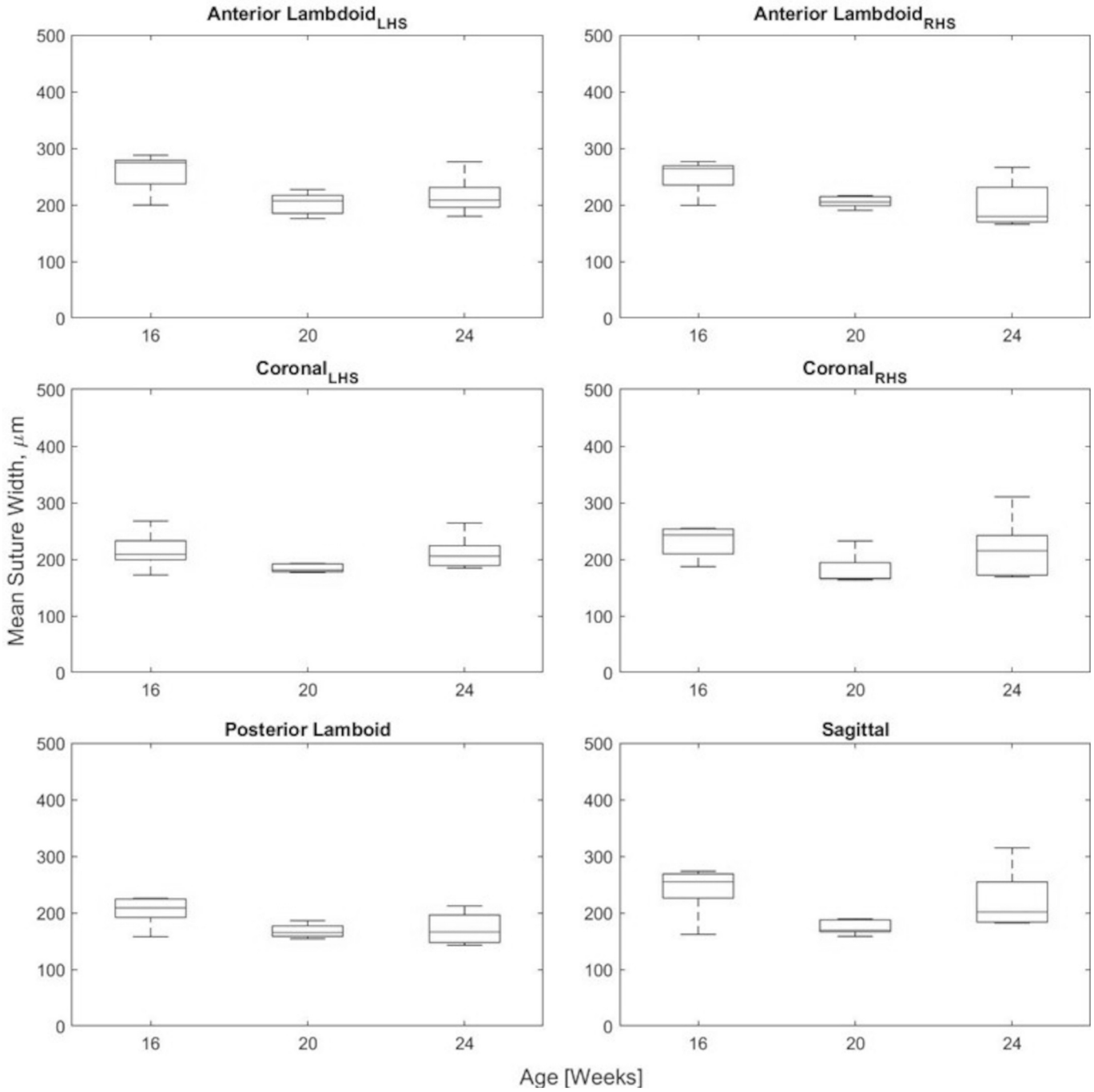

Fig. 14. Mean suture width boxplots for suture regions of interest, grouped by age (16, 20, 24 week-of-age). LHS = left-hand side, RHS = right-hand side.

Table 1
Test statistics, H, relating mean suture linear interdigitation index (LII) and mean suture width between rat age groups determined using Kruskal-Wallis tests. PL = posterior lambdoid, AL RHS = right-hand side anterior lambdoid, AL LHS = left-hand side anterior lambdoid, S = sagittal, C RHS = right-hand side coronal, C LHS = left-hand side coronal.

Suture	H, suture LII	H, mean suture width
PL	1.01	3.75
AL RHS	6.86	4.46
AL LHS	2.88	3.78
S	0.42	4.58
C RHS	0.74	5.18
C LHS	0.74	3.86

as a full plane of suture was required to perform the analysis. Including this would improve the range of analysis of the study. Finally, the utilized dataset only considered a limited sample size of female rats. Future work considering a larger sample size with male and female subjects would be beneficial towards improved statistical power and the study of sex related differences in suture morphometry/development. Despite these limitations, the presented work demonstrated the utility of a novel approach to studying suture morphometry with respect to width and LII, where through-thickness differences were noted in both variables and across different sutures of the skull in a quantitative manner. The results of this work should prompt researchers interested in suture development, mechanics, morphology, and modelling to consider how this variability affects results based on the complexity metrics being used.

Table 2
The *p*-values of multiple nonparametric comparisons between suture linear interdigitation indices (LII). PL = posterior lambdoid, AL RHS = right-hand side anterior lambdoid, AL LHS = left-hand side anterior lambdoid, S = sagittal, C RHS = right-hand side coronal, C LHS = left-hand side coronal.

Pairwise suture comparisons		*p*-Value
PL	AL RHS	0.128
PL	AL LHS	0.146
PL	S	0.810
PL	C RHS	0.007**
PL	C LHS	0.025*
AL RHS	AL LHS	>0.999
AL RHS	S	<0.000**
AL RHS	C RHS	0.999
AL RHS	C LHS	>0.999
AL LHS	S	<0.000**
AL LHS	C RHS	0.998
AL LHS	C LHS	>0.999
S	C RHS	<0.000**
S	C LHS	<0.000**
C RHS	C LHS	>0.999

* <0.05.
** <0.01.

5. Conclusions

The image analysis results showed variations in local planar widths, mean planar widths, and planar LII through the thickness of the skull of individual sutures. The data shown regarding mean planar widths, planar LII, and sutures centerlines through the skull thickness highlighted the 3D variability of cranial suture morphology. In the sutures analyzed, suture width and LII between different aged animals was largely found to be statistically insignificant. Future works related to this study could include single animal 3D morphometric development analysis, in vivo 3D morphological analysis to applied loading, increasing sample sizes, increasing the age range, and/or analyzing different species. If researchers are interested in suture morphometry, measures should be taken to account for 3D suture morphology.

CRediT authorship contribution statement

Ross Remesz: Writing – review & editing, Writing – original draft, Methodology, Investigation, Formal analysis, Data curation, Conceptualization. **Tsolmonbaatar Khurelbaatar:** Writing – review & editing, Methodology, Investigation, Formal analysis. **Karyne N. Rabey:** Writing – review & editing, Methodology, Investigation, Formal analysis, Conceptualization. **Michael R. Doschak:** Writing – review & editing, Supervision, Methodology, Investigation, Funding acquisition, Formal analysis, Conceptualization. **Dan L. Romanyk:** Writing – review & editing, Supervision, Methodology, Investigation, Funding acquisition, Formal analysis, Conceptualization.

Declaration of competing interest

The authors declare that they have no known competing financial interests or personal relationships that could have appeared to influence the work reported in this paper.

Data availability

Data will be made available on request.

Acknowledgements

This work was supported in part by the NSERC Discovery Grant, NFRF Exploration, and the Geoffrey and Robyn Sperber Craniofacial Biology Research funding programs. The authors have no competing interest to declare.

References

Bishara, S.E., Staley, R.N., 1987. Maxillary expansion: clinical implications. Am. J. Orthod. Dentofacial Orthop. 91, 3–14.
Burn, A.K., et al., 2010. Dietary consistency and the midline sutures in growing pigs. Orthodontics Craniofacial Res. 13, 106–113.
Byron, C.D., 2006. Role of the osteoclast in cranial suture waveform patterning. Anatatomical Record - Part A. Discov. Mol. Cell. Evol. Biol. 288, 552–563.
Byron, C.D., 2009. Cranial suture morphology and its relationship to diet in cebus. J. Hum. Evol. 57, 649–655.
Cohen, M.M., 1993. Sutural biology and the correlates of craniosynostosis. Am. J. Med. Genet. 47, 581–616.
Dunn, O.J., 1961. Multiple comparisons among means. J. Am. Stat. Assoc. 56 (293), 52–64.
Guerrero-vargas, J.A., Silva, T.A., Macari, S., Casas, E.B.D. Las, Garzón-alvarado, D.A., 2019. Influence of interdigitation and expander type in the mechanical response of the midpalatal suture during maxillary expansion. Comput. Methods Programs Biomed. 176, 195–209.
Henderson, J.H., Chang, L.Y., Song, H.J.M., Longaker, M.T., Carter, D.R., 2005. Age-dependent properties and quasi-static strain in the rat sagittal suture. J. Biomech. 38, 2294–2301.
Herring, S.W., 2008. Mechanical influences on suture development and patency. Front. Oral Biol. 12, 41–56.
Herring, S.W., Mucci, R.J., 1991. In vivo strain in cranial sutures: the zygomatic arch. J. Morphol. 207, 225–239.
Herring, S.W., Ochareon, P., 2005. Bone – special problems of the craniofacial region. Orthodontics Craniofacial Res. 8, 174–182.
Hughes, P.C., Tanner, J.M., 1970. The assessment of skeletal maturity in the growing rat. J. Anat. 106, 371–402.
Jasinoski, S.C., Reddy, B.D., 2012. Mechanics of cranial sutures during simulated cyclic loading. J. Biomech. 45, 2050–2054.
Jasinoski, S.C., Reddy, B.D., Louw, K.K., Chinsamy, A., 2010. Mechanics of cranial sutures using the finite element method. J. Biomech. 43, 3104–3111.
Jaslow, C.R., 1990. Mechanical properties of cranial sutures. J. Biomech. 23, 313–321.
Jayaprakash, P.T., Srinivasan, G.J., 2013. Skull sutures: changing morphology during preadolescent growth and its implications in forensic identification. Forensic Sci. Int. 229, 166.e1–166.e13.
Khonsari, R.H., Di Rocco, F., Arnaud, É., Sanchez, S., Tafforeau, P., 2012. High-resolution imaging of craniofacial sutures: new tools for understanding the origins of craniosynostoses. Childs Nerv. Syst. 28, 1465–1469.
Liu, L., et al., 2017. The effects of morphological irregularity on the mechanical behavior of interdigitated biological sutures under tension. J. Biomech. 58, 71–78.
Maloul, A., Fialkov, J., Whyne, C.M., 2013. Characterization of the bending strength of craniofacial sutures. J. Biomech. 46, 912–917.
Maloul, A., Fialkov, J., Wagner, D., Whyne, C.M., 2014. Characterization of craniofacial sutures using the finite element method. J. Biomech. 47, 245–252.
Mao, J.J., Wang, X., Kopher, R.A., 2003. Biomechanics of craniofacial sutures: orthopedic implications. Angle Orthod. 73, 128–135.
Markey, M.J., Marshall, C.R., 2007. Linking form and function of the fibrous joints in the skull: a new quantification scheme for cranial sutures using the extant fish polypt. J. Morphol. 268, 89–102.
Markey, M.J., Main, R.P., Marshall, C.R., 2006. In vivo cranial suture function and suture morphology in the extant fish Polypterus: implications for inferring skull function in living and fossil fish. J. Exp. Biol. 209, 2085–2102.
Nicolay, C.W., Vaders, M.J., 2006. Cranial suture complexity in white-tailed deer (Odocoileus virginianus). J. Morphol. 267, 841–849.
Opperman, L.A., 2000. Cranial sutures as intramembranous bone growth sites. Dev. Dyn. 219, 472–485.
Panahifar, A., et al., 2014. Development and reliability of a multi-modality scoring system for evaluation of disease progression in pre-clinical models of osteoarthritis: celecoxib may possess disease-modifying properties. Osteoarthr. Cartil. 22, 1639–1650.
Peptan, A.I., Lopez, A., Kopher, R.A., Mao, J.J., 2008. Responses of intramembranous bone and sutures upon in vivo cyclic tensile and compressive loading. Bone 42, 432–438.
Persson, M., 1995. The role of sutures in normal and abnormal craniofacial growth. Acta Odontol. Scand. 53, 152–161.
Radhakrishnan, P., Mao, J.J., 2004. Nanomechanical properties of facial sutures and sutural mineralization front. J. Dent. Res. 83, 470–475.
Rafferty, K.L., Herring, S.W., 1999. Craniofacial sutures: morphology, growth, and in vivo masticatory strains. J. Morphol. 242, 167–179.
Rafferty, K.L., Herring, S.W., Marshall, C.D., 2003. Biomechanics of the rostrum and the role of facial sutures. J. Morphol. 257, 33–44.
Rafferty, K.L., Baldwin, M.C., Soh, S.H., Herring, S.W., 2019. Mechanobiology of bone and suture – results from a pig model. Orthod. Craniofacial Res. 22, 82–89.
Savoldi, F., Xu, B., Tsoi, J.K.H., Paganelli, C., Matinlinna, J.P., 2018. Anatomical and mechanical properties of swine midpalatal suture in the premaxillary, maxillary, and palatine region. Sci. Rep. 8, 1–12.
Savoldi, F., Tsoi, J.K.H., Paganelli, C., Matinlinna, J.P., 2019. Sutural morphology in the craniofacial skeleton: a descriptive microcomputed tomography study in a swine model. Anat. Rec. 302, 2156–2163.
Sheskin, D., 2011. Handbook of Parametric and Nonparametric Statistical Procedures, A Chapman & Hall Book.

Šidák, Z., 1967. Rectangular confidence regions for the means of multivariate normal distributions. J. Am. Stat. Assoc. 62, 626–633.
Soh, S.H., Rafferty, K., Herring, S., 2018. Cyclic loading effects on craniofacial strain and sutural growth in pigs. Am. J. Orthod. Dentofacial Orthop. 154, 270–282.
Sun, Z., Lee, E., Herring, S.W., 2004. Cranial sutures and bones: growth and fusion in relation to masticatory strain. Anat. Rec. A Discov. Mol. Cell. Evol. Biol. 276, 150–161.
Vij, K., Mao, J.J., 2006. Geometry and cell density of rat craniofacial sutures during early postnatal development and upon in vivo cyclic loading. Bone 38, 722–730.
Willershausen, I., et al., 2019. Development of a novel histological and histomorphometric evaluation protocol for a standardized description of the mid-palatal suture – an ex vivo study. J. Anat. 235, 180–188.
Wu, B.H., et al., 2017. Stretch force guides finger-like pattern of bone formation in suture. PloS One 12, 1–15.
Yu, J.C., Borke, J.L., Zhang, G., 2004. Brief synopsis of cranial sutures: optimization by adaptation. Semin. Pediatr. Neurol. 11 (4), 249–255. https://doi.org/10.1016/j.spen.2004.10.002.